Hindawi Publishing Corporation
International Journal of Photoenergy
Volume 2016, Article ID 2047591, 6 pages
http://dx.doi.org/10.1155/2016/2047591

Research Article

Indium-Free PTB7/$PC_{71}BM$ Polymer Solar Cells with Solution-Processed Al:ZnO Electrodes on PET Substrates

P. Fuchs,[1] A. Paracchino,[2] H. Hagendorfer,[1] L. Kranz,[1] T. Geiger,[2] Y. E. Romanyuk,[1] A. N. Tiwari,[1] and F. Nüesch[2]

[1]*Laboratory for Thin Films and Photovoltaics, Swiss Federal Laboratories for Material Science and Technology (Empa), Ueberlandstrasse 129, 8600 Dübendorf, Switzerland*
[2]*Laboratory for Functional Polymers, Swiss Federal Laboratories for Material Science and Technology (Empa), Ueberlandstrasse 129, 8600 Dübendorf, Switzerland*

Correspondence should be addressed to P. Fuchs; peter.fuchs@empa.ch

Received 30 October 2015; Revised 3 February 2016; Accepted 10 February 2016

Academic Editor: Giuseppe Portale

Inverted PTB7/$PC_{71}BM$ polymer solar cells are prepared on solution-processed Al:ZnO transparent contacts on PET substrates. Al:ZnO is deposited by a low temperature chemical bath deposition route ($T < 100^{\circ}C$ at any step) to comply with the temperature sensitive substrate. A maximum conversion efficiency of 6.4% and 6.9% is achieved for the indium-free solar cells on PET and glass substrates, respectively. The devices are relatively stable in air whereby an initial efficiency loss in the order of 15% after storage for 15 days can be fully recovered by light soaking.

1. Introduction

Major improvements have been made in the field of organic photovoltaics (OPV) since the first works in 1995 [1, 2]. Molecular engineering brought up a series of push-pull copolymers with narrow band gaps in the range of 1-2 eV and low-lying Highest Occupied Molecular Orbital (HOMO) level for increased light harvesting and open-circuit potential [3]. The efficiency of organic solar cells (OSCs) strongly depends on the morphology of the polymer-fullerene network, which in turn depends on thermal treatments and on the presence of additives in the polymer blend solution [4, 5]. Likewise interfacial buffer layers between the organic layer and the metal electrodes, notably metal oxides, self-assembled monolayers (SAM), and conjugated polyelectrolytes (CPE) improve the efficiency and stability of OSCs [6, 7]. In case of metal oxides wide-bandgap interfacial layers (e.g., MoO_3, WO_3, ZnO, and TiO_2) provide ohmic contacts for electrons or holes, being blocking layers for the charge carriers of opposite sign. Further they bolster device stability, for example, by stopping diffusion of metal atoms from the electrodes into the organic layer and finally work as optical spacers to enhance the light absorption in the active layer [8, 9]. In this respect, it would be of interest if such oxide layers can also act as barrier layers for air and moisture, to significantly increase stability and ease the handling and production of OSC based solar cell devices.

A typical OSC consists of an electron-donor polymer and an electron-acceptor fullerene-derivative blend as absorber sandwiched between a transparent conducting window layer and hole extraction layer with work functions carefully matched (Figures 1(a) and 1(b)). In the case of OSCs in the inverted geometry, the window layer is commonly a stack of indium tin oxide (ITO) and ZnO or TiO_2 to combine good conductivity (from the ITO layer) and appropriate band gap matching (from the ZnO or TiO_2 layer) [6]. With respect to the limited indium supply, the ITO layer would ideally be replaced by a doped ZnO layer. Doped ZnO thin films can be synthesized by sol-gel based methods but to achieve suitable electronic conductivity an annealing step at $400^{\circ}C$ or higher is typically required [10], which is not compatible with most polymer substrates (preferably processing temperatures $< 120^{\circ}C$ for low cost polymers such as PET). Sol-gel procedures at lower process temperatures ($140^{\circ}C$–$260^{\circ}C$) result in lower electrical performances and thus require the use of ITO to compensate for the insufficient

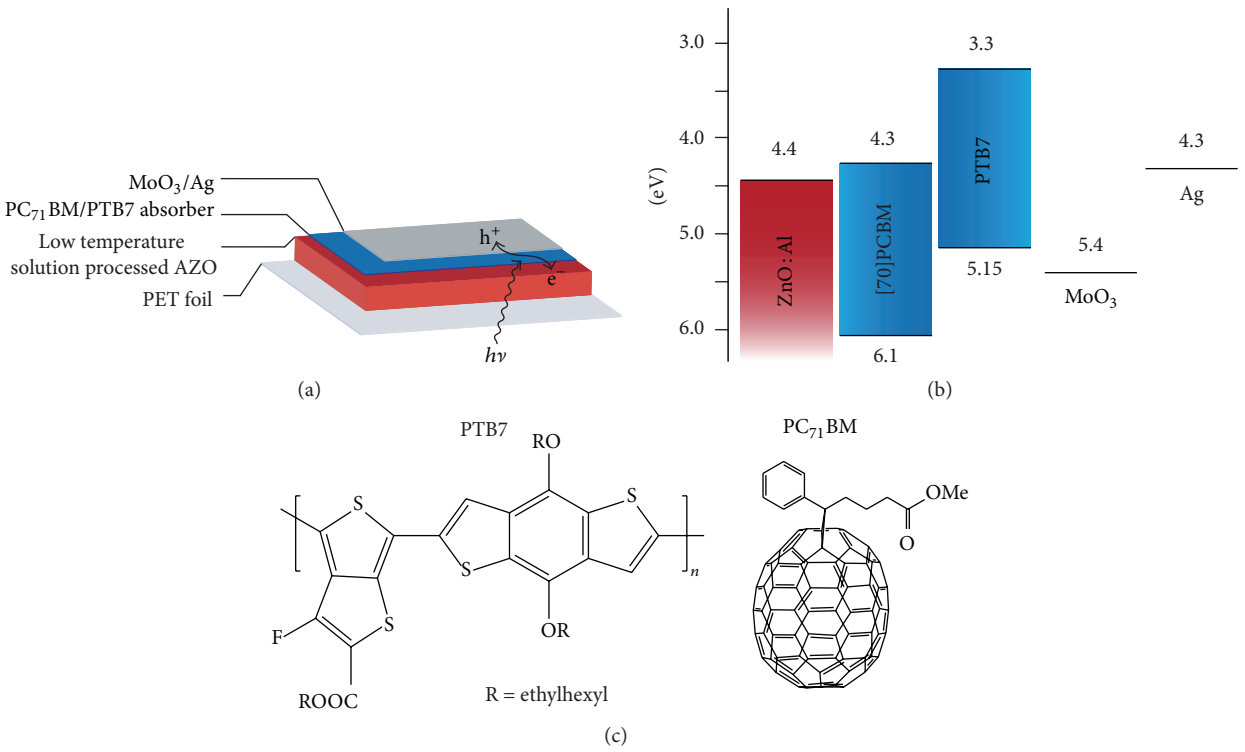

FIGURE 1: (a) Schematic view of the device architecture. (b) Vacuum energy level diagram for each material used in this study. (c) Chemical structure of the polymer donor PTB7 and the fullerene-derivative $PC_{71}BM$.

conductivity [11–14]. To overcome this bottleneck a recently reported low temperature aqueous solution process using chemical bath deposition (CBD) is applied in this work to deposit adherent, transparent, and conductive Al:ZnO (AZO) thin films on PET [15]. Furthermore the air stability of the resulting devices is examined over a few days.

2. Materials and Methods

2.1. Preparation of AZO/PET Substrates. PET foils (Melinex® ST504™ films by DuPont Teijin) were Ar-plasma cleaned for 5 minutes (Diener Femto, low pressure plasma system) for a better adherence of the AZO layer and fixed in a metal frame for further processing. The seed layer (required for heterogeneous nucleation, 60–80 nm intrinsic ZnO) used for systematic investigations of the CBD deposition and the AZO layer for the reference cells (500 nm, Al doping of 2 at% relative to Zn) were deposited using RF-magnetron sputtering at room temperature. For complete nonvacuum and low temperature processing the ZnO seed layer was prepared by spin or dip coating of an AZO nanoparticle dispersion (10 mg mL^{-1}) in ethanol (3000 rpm, 30 sec, 2x) and drying on a hotplate at 80°C for 2 min resulting in 60–80 nm thick layers. The AZO nanoparticles were synthesized by a microwave-assisted nonaqueous sol-gel method [16].

The precursor solution was prepared as previously reported in [15]: ammonium citrate (2 mM), ammonium nitrate (50 mM), and ZnO powder (50 mM) were dissolved/suspended in 0.97 M ammonium hydroxide. The solution was stirred overnight and filtered (1 μm glass fiber filter). The filtered solution is preheated for 15 min in a circulated heating bath at a set temperature of 90°C, resulting in deposition solution temperature of ~80°C. Chemical bath deposition of AZO then took place at a deposition temperature of ~80°C for 1 h. Al doping was conducted by coprecipitation, whereby Al ions were introduced into the solution by the immersion/corrosion of an Al foil (see [15]). After deposition the substrate was washed with deionised water and dried in a N_2 stream.

To enhance the electrical conductivity, a 10 min UV radiation treatment was performed using a 250 W UV-handheld apparatus (Hoenle UV technology, 5 cm distance to substrate, 70 mW cm^{-2} UVA) with an iron doped Hg lamp so that substrate temperature did not exceed 80°C.

2.2. Fabrication of Solar Cells. The PET/AZO substrates were ultrasonicated for 1 minute in water and isopropanol and dried in a nitrogen flow. The electron-donor PTB7 and the electron-acceptor $PC_{71}BM$ (99%) were purchased from 1-material and Solenne, respectively. The polymer blend was prepared in a glovebox as follows: two separate solutions of 12 mg mL^{-1} of PTB7 and 36 mg mL^{-1} of $PC_{71}BM$ were stirred for few hours at 60°C and then mixed in the volume ratio 2 : 1. 3% vol of 1,8-diiodoctane was added to the blend that was further stirred for one hour. The solution was passed through a 0.45 μm filter and spin-coated while still warm at 1000 rpm. The active layer thickness was between 85 and 95 nm. The hole extraction layer consisted of 15 nm of thermally evaporated MoO_3 (Sigma Aldrich 99.99%). Cells were completed by evaporating Ag (Cerac, 99.99%)

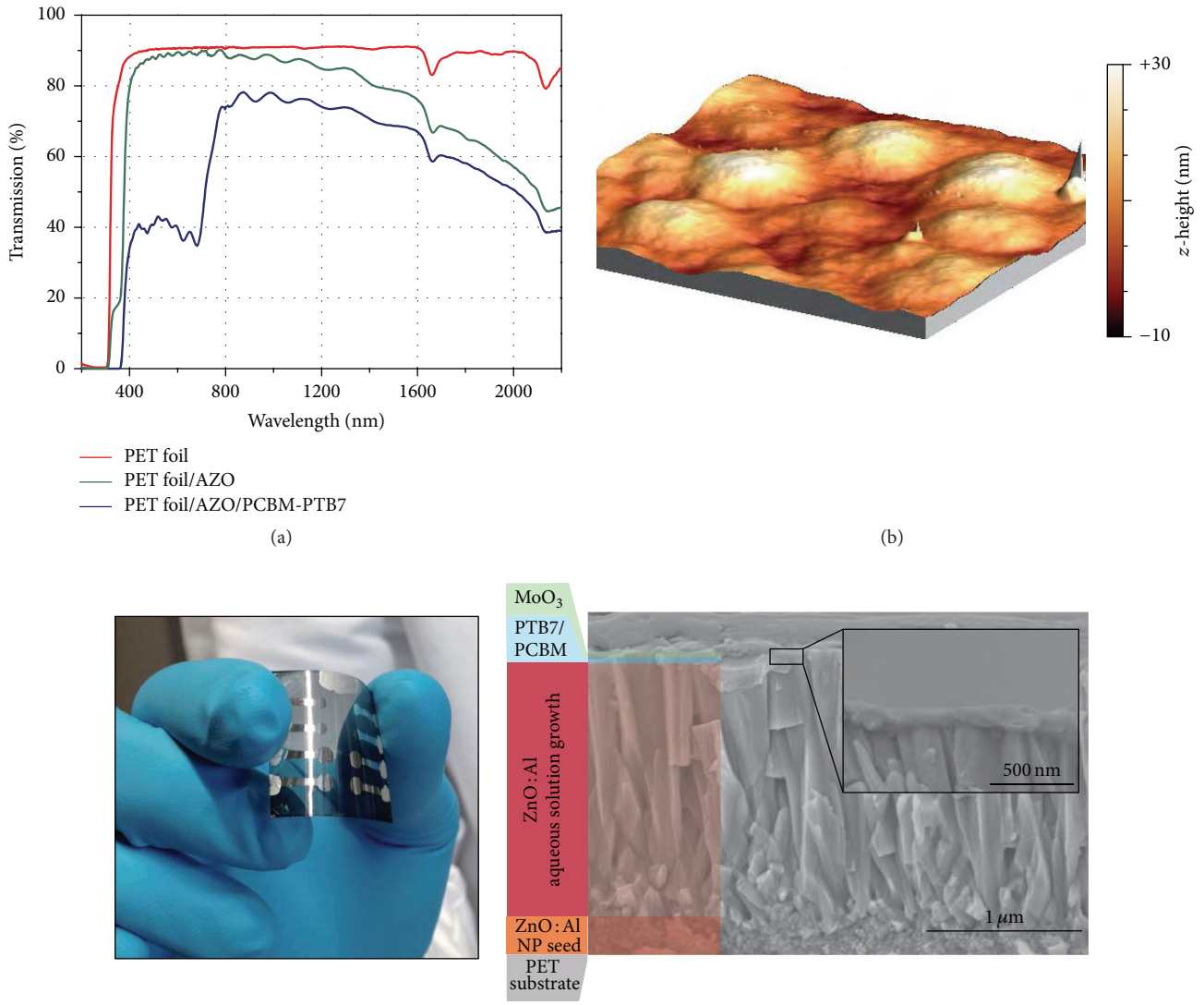

Figure 2: (a) UV-Vis transmission spectrum of CBD-AZO on PET and of the photoactive layer on CBD-AZO. (b) AFM topography measurements of an AZO layer on PET foil ($2 \times 2\,\mu$m). (c) Photograph of solar cells with solution-processed AZO on PET polymer foil substrate. (d) SEM cross section of the device on PET foil.

electrodes (80 nm) through a shadow mask defining eight cells per substrate. The thermal evaporations were carried out in the same vacuum chamber (5×10^{-6} mbar) with a deposition rate of 0.2 Å s^{-1} for MoO_3 and up to 2 Å s^{-1} for Ag.

2.3. Characterization and Measurements. An air-tight transfer box was used to measure the *J-V* characteristics outside the glove box on a calibrated solar simulator (Spectra Nova) using a Xe lamp with 100 mW cm^{-2} simulated AM1.5 solar irradiation. The cell area was between 5 and 7 mm^2. The external quantum efficiency (EQE) of the solar cells was measured with a lock-in amplifier. A chopped white light source (900 W halogen lamp, 360 Hz) and a dual grating monochromator generated the probing beam. A certified monocrystalline Si cell was used as the reference cell. Absorbance was measured with a Varian Cary 50 using a glass substrate as baseline and transmittance with a Shimadzu UV-3600 UV-Vis spectrophotometer using air as baseline.

3. Results and Discussion

Adherent and transparent CBD-AZO layers (Figure 2(a)) were applied on PET substrates resulting in a sheet resistance of ~40 Ωsq for 1.5–2 μm thick films. CBD-AZO films on PET exhibited a rms roughness of 5.8 nm (Figure 2(b)). Such a smooth surface permitted direct spin coating of the photoactive layer on top. The photoactive layer of choice (Figure 1(c)) consists of a blend of [6, 6]-phenyl C71-butyric acid methyl ester ($PC_{71}BM$) and the low-bandgap semiconducting polythieno[3,4-b]thiophene-co-benzodithiophene (PTB7). MoO_3 is used as hole extraction layer. When exposed to air after deposition, a change of surface stoichiometry lowers the

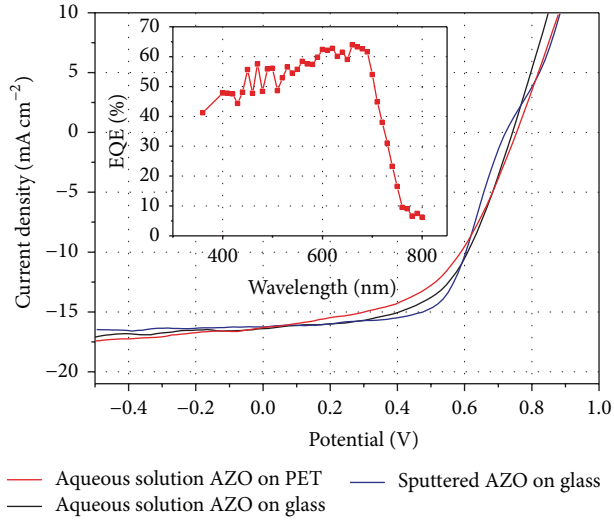

(a)

Device type	V_{oc} (V)	J_{sc} (mA/cm^2)	FF (%)	PCE (%)
Sputtered/glass	0.73	16.6	62.7	7.6
CBD/glass	0.74	16.5	57.6	6.9
CBD/PET	0.75	16.4	52.2	6.4

(b)

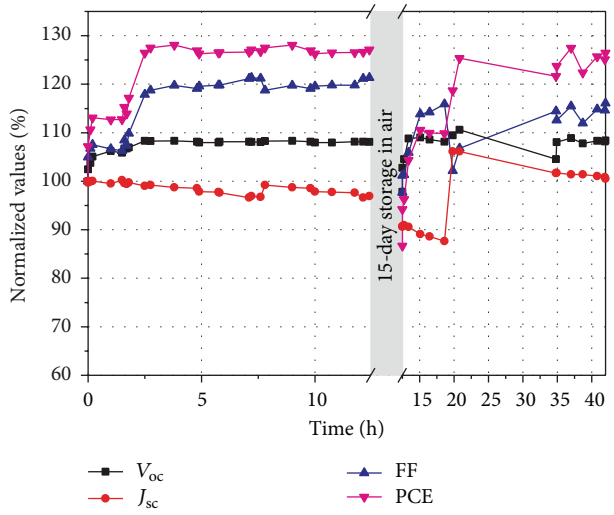

(c)

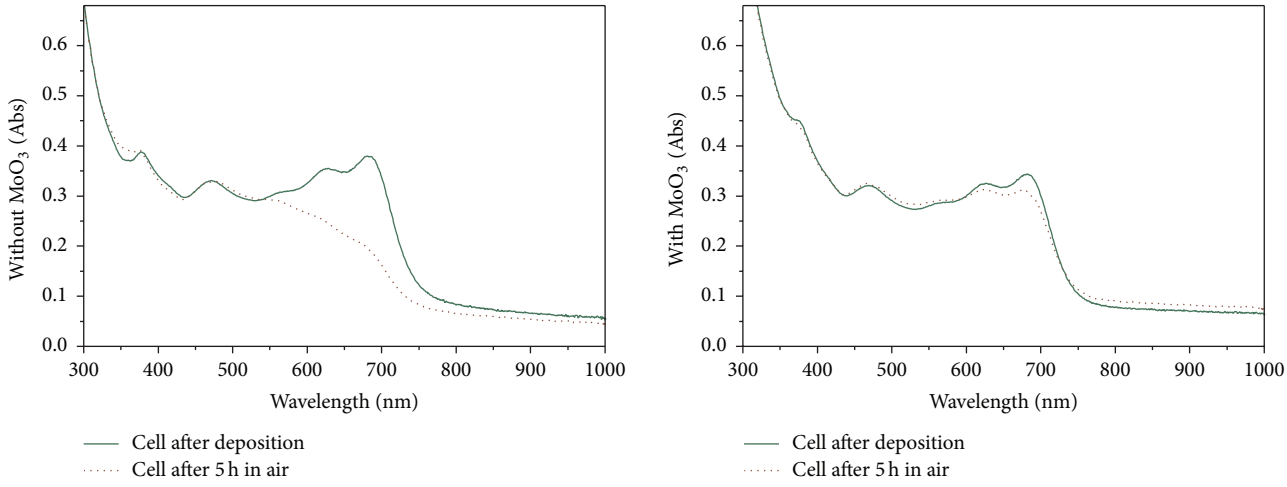

(d)

Figure 3: (a) Current-voltage curves for the best devices with AZO sputtered on glass, solution deposited AZO on glass, and solution-processed AZO on PET foil. Inset: external quantum efficiency (EQE) for a cell on PET foil. (b) Photovoltaic parameters for the curves in (a). (c) Stability under AM1.5 irradiation in air. (d) Normal incidence absorbance spectra of the active layer with and without a MoO_3 (15 nm) top layer before (solid curves) and after 5-hour irradiation in air (dotted curves). The interference fringes are due to the AZO layer.

work function of MoO_3 from −6.9 eV to about −5.4 eV, providing a good energy alignment to the HOMO level of most electron-donor polymers [17]. Recent publications demonstrated that solution-processed MoO_3 can replace thermally evaporated MoO_3 in organic solar cells, thanks to the similar work-function value [18–23]. Furthermore increased stability has been reported when employing a MoO_3 top layer [24]. Thus, already a few nanometer thin layer can serve as a hole extraction layer and protective layer at once.

A photograph and SEM cross section of the final device are presented in Figures 2(c) and 2(d). The current-voltage curves and the photovoltaic parameters for devices with a RF-magnetron sputtered AZO reference (500 nm, 25 Ωsq) on glass and CBD-AZO on glass and PET are shown in Figures 3(a) and 3(b), respectively. For the reference cell the power conversion efficiency (PCE) was 7.6% for the best device, with an average value of 6.8% ($n = 6$). The device with AZO deposited by the aqueous solution process showed a lower shunt resistance and therefore a lower fill factor (FF). The cells reached 6.9% with an average value of 5.2% ($n = 6$). The best cell on PET reached 6.4% PCE. As compared to the sputtered AZO, the fairly thick edge of the solution deposited AZO might be difficult to coat with the thin active layer (80–90 nm), creating alternative current pathways. However, this problem could be solved in a module design with adequate stack geometry.

The polymer PTB7, as benzo-dithiophene-based conjugated polymers in general, has been reported to be unstable when exposed to oxygen and light with an irreversible color change from blue to yellow [25, 26]. This is due to a photochemical reaction of the benzodithiophene unit with oxygen molecules at the excited state, causing the disruption of the conjugation system. Consequently, degradation is not expected to occur if the polymer is sandwiched between two continuous oxygen barrier layers. AZO and MoO_3 can effectively serve this function, the latter being only 15 nm thick. In previous works, stability under air storage, and not under working conditions, was investigated for cells with inverted and regular geometry [24, 27, 28]. To simulate more realistic conditions the stability under illumination and air simultaneously is tested. As shown in Figure 3(c), a rapid increase of V_{oc} goes along with a progressively disappearing S-shape in the *IV* curve after the first minutes of irradiation. Over time also FF and PCE greatly increase exceeding 120% of the initial value after 2.5 hours and being constant upon further illumination. In contrast, the short circuit current (J_{sc}) decreased slightly over time, maintaining 97% of the initial value after 10 hours of illumination. After a period of storage in air under ambient light, the S-shape was recovered and again gradually disappeared under illumination. This improvement most likely arises from the enhanced conductivity of one or both of the metal oxides films under light, due to trap filling or photodoping [8, 29].

This results in an improvement of the electronic interface between one or both metal oxides and the organic material, reducing charge accumulation at the metal oxide/organic interface suppressing the S-shape. Due to the similar value of bandgap of MoO_3 and ZnO and the fact that light enters the device from the AZO side, no UV light is expected to hit the MoO_3 film. Thus the improvement in the energy alignment likely occurs at the AZO/organic interface.

Despite the stable photovoltaic performance of the devices, in the region of the substrate not covered by the MoO_3 thin layer, a color change from the initial green color of the donor-acceptor blend to ochre was observed already after a few hours of irradiation. This is confirmed by the absorbance spectra (Figure 3(d)) where unprotected PTB7:PCBM blend exhibits a reduction of the PTB7 absorption peaks at 620 and 680 nm. The color stayed unaltered where MoO_3 was present, indicating that MoO_3 protected the polymer underneath against the photochemical degradation.

4. Conclusions

Al:ZnO was grown at low temperature on PET substrates and combined with organic PTB7/$PC_{71}BM$ absorber layers to form indium-free OPV devices with an efficiency up to 6.4%. Both the 15 nm thin MoO_3 back contact and the 1.5–2 μm thick AZO front contact were effectively serving as a moisture barrier when storing the device for 15 days in air.

Competing Interests

The authors declare that they have no competing interests.

Authors' Contributions

P. Fuchs, A. Paracchino, and H. Hagendorfer have contributed equally to the work.

Acknowledgments

Financial support from the Swiss National Science Foundation (SNF-NanoTera) and Swiss Federal Office of Energy (SYNERGY) and CCEM CONNECT-PV is gratefully acknowledged.

References

[1] J. J. M. Halls, C. A. Walsh, N. C. Greenham et al., "Efficient photodiodes from interpenetrating polymer networks," *Nature*, vol. 376, no. 6540, pp. 498–500, 1995.

[2] G. Yu, J. Gao, J. C. Hummelen, F. Wudl, and A. J. Heeger, "Polymer photovoltaic cells: enhanced efficiencies via a network of internal donor-acceptor heterojunctions," *Science*, vol. 270, no. 5243, pp. 1789–1791, 1995.

[3] P.-L. T. Boudreault, A. Najari, and M. Leclerc, "Processable low-bandgap polymers for photovoltaic applications," *Chemistry of Materials*, vol. 23, no. 3, pp. 456–469, 2011.

[4] W. Ma, C. Yang, X. Gong, K. Lee, and A. J. Heeger, "Thermally stable, efficient polymer solar cells with nanoscale control of the interpenetrating network morphology," *Advanced Functional Materials*, vol. 15, no. 10, pp. 1617–1622, 2005.

[5] K. R. Graham, R. Stalder, P. M. Wieruszewski, D. G. Patel, D. H. Salazar, and J. R. Reynolds, "Tailor-made additives for morphology control in molecular bulk-heterojunction photovoltaics," *ACS Applied Materials and Interfaces*, vol. 5, no. 1, pp. 63–71, 2013.

[6] S. Chen, J. R. Manders, S.-W. Tsang, and F. So, "Metal oxides for interface engineering in polymer solar cells," *Journal of Materials Chemistry*, vol. 22, no. 46, pp. 24202–24212, 2012.

[7] J. H. Seo, A. Gutacker, Y. Sun et al., "Improved high-efficiency organic solar cells via incorporation of a conjugated polyelectrolyte interlayer," *Journal of the American Chemical Society*, vol. 133, no. 22, pp. 8416–8419, 2011.

[8] G. Williams, Q. Wang, and H. Aziz, "The photo-stability of polymer solar cells: contact photo-degradation and the benefits of interfacial layers," *Advanced Functional Materials*, vol. 23, no. 18, pp. 2239–2247, 2013.

[9] A. K. K. Kyaw, D. H. Wang, D. Wynands et al., "Improved light harvesting and improved efficiency by insertion of an optical spacer (ZnO) in solution-processed small-molecule solar cells," *Nano Letters*, vol. 13, no. 8, pp. 3796–3801, 2013.

[10] M. Ohyama, H. Kozuka, and T. Yoko, "Sol-gel preparation of ZnO films with extremely preferred orientation along (002) plane from zinc acetate solution," *Thin Solid Films*, vol. 306, no. 1, pp. 78–85, 1997.

[11] T. Stubhan, H. Oh, L. Pinna, J. Krantz, I. Litzov, and C. J. Brabec, "Inverted organic solar cells using a solution processed aluminum-doped zinc oxide buffer layer," *Organic Electronics*, vol. 12, no. 9, pp. 1539–1543, 2011.

[12] J. Min, H. Zhang, T. Stubhan et al., "A combination of Al-doped ZnO and a conjugated polyelectrolyte interlayer for small molecule solution-processed solar cells with an inverted structure," *Journal of Materials Chemistry A*, vol. 1, no. 37, pp. 11306–11311, 2013.

[13] T. Stubhan, I. Litzov, N. Li et al., "Overcoming interface losses in organic solar cells by applying low temperature, solution processed aluminum-doped zinc oxide electron extraction layers," *Journal of Materials Chemistry A*, vol. 1, no. 19, pp. 6004–6009, 2013.

[14] T. Stubhan, M. Salinas, A. Ebel et al., "Increasing the fill factor of inverted P3HT:PCBM solar cells through surface modification of al-doped ZnO via phosphonic acid-anchored C60 SAMs," *Advanced Energy Materials*, vol. 2, no. 5, pp. 532–535, 2012.

[15] H. Hagendorfer, K. Lienau, S. Nishiwaki et al., "Highly transparent and conductive ZnO: Al thin films from a low temperature aqueous solution approach," *Advanced Materials*, vol. 26, no. 4, pp. 632–636, 2013.

[16] L. Luo, M. D. Rossell, D. Xie, R. Erni, and M. Niederberger, "Microwave-assisted nonaqueous sol-gel synthesis: from Al:ZnO nanoparticles to transparent conducting films," *ACS Sustainable Chemistry and Engineering*, vol. 1, no. 1, pp. 152–160, 2013.

[17] I. Irfan, A. James Turinske, Z. Bao, and Y. Gao, "Work function recovery of air exposed molybdenum oxide thin films," *Applied Physics Letters*, vol. 101, no. 9, Article ID 093305, pp. 8–12, 2012.

[18] C. Girotto, E. Voroshazi, D. Cheyns, P. Heremans, and B. P. Rand, "Solution-processed MoO_3 thin films as a hole-injection layer for organic solar cells," *ACS Applied Materials and Interfaces*, vol. 3, no. 9, pp. 3244–3247, 2011.

[19] S. R. Hammond, J. Meyer, N. E. Widjonarko et al., "Low-temperature, solution-processed molybdenum oxide hole-collection layer for organic photovoltaics," *Journal of Materials Chemistry*, vol. 22, no. 7, pp. 3249–3254, 2012.

[20] J. J. Jasieniak, J. Seifter, J. Jo, T. Mates, and A. J. Heeger, "A solution-processed MoOx anode interlayer for use within organic photovoltaic devices," *Advanced Functional Materials*, vol. 22, no. 12, pp. 2594–2605, 2012.

[21] J. Liu, X. Wu, S. Chen et al., "Low-temperature MoO_3 film from a facile synthetic route for an efficient anode interfacial layer in organic optoelectronic devices," *Journal of Materials Chemistry C*, vol. 2, no. 1, pp. 158–163, 2014.

[22] S. Murase and Y. Yang, "Solution processed MoO 3 interfacial layer for organic photovoltaics prepared by a facile synthesis method," *Advanced Materials*, vol. 24, no. 18, pp. 2459–2462, 2012.

[23] K. Zilberberg, H. Gharbi, A. Behrendt, S. Trost, and T. Riedl, "Low-temperature, solution-processed MoO_x for efficient and stable organic solar cells," *ACS Applied Materials and Interfaces*, vol. 4, no. 3, pp. 1164–1168, 2012.

[24] M. J. Tan, S. Zhong, J. Li, Z. Chen, and W. Chen, "Air-stable efficient inverted polymer solar cells using solution-processed nanocrystalline ZnO interfacial layer," *ACS Applied Materials and Interfaces*, vol. 5, no. 11, pp. 4696–4701, 2013.

[25] S. Alem, S. Wakim, J. Lu, G. P. Robertson, J. Ding, and Y. Tao, "Degradation mechanism of benzodithiophene-based conjugated polymers when exposed to light in air," *ACS Applied Materials & Interfaces*, vol. 4, no. 6, pp. 2993–2998, 2012.

[26] Y. W. Soon, H. Cho, J. Low, H. Bronstein, I. McCulloch, and J. R. Durrant, "Correlating triplet yield, singlet oxygen generation and photochemical stability in polymer/fullerene blend films," *Chemical Communications*, vol. 49, no. 13, pp. 1291–1293, 2013.

[27] S. Woo, W. Hyun Kim, H. Kim, Y. Yi, H.-K. Lyu, and Y. Kim, "8.9% single-stack inverted polymer solar cells with electron-rich polymer nanolayer-modified inorganic electron-collecting buffer layers," *Advanced Energy Materials*, vol. 4, no. 7, Article ID 1301692, pp. 1–7, 2014.

[28] Y. Sun, C. J. Takacs, S. R. Cowan et al., "Efficient, air-stable bulk heterojunction polymer solar cells using MoOx as the anode interfacial layer," *Advanced Materials*, vol. 23, no. 19, pp. 2226–2230, 2011.

[29] H. Zhang, A. Borgschulte, F. A. Castro et al., "Photochemical transformations in fullerene and molybdenum oxide affect the stability of bilayer organic solar cells," *Advanced Energy Materials*, vol. 5, no. 2, Article ID 1400734, pp. 1–9, 2015.